




Research Article

Observation of CCNR-type electrical switching in $\text{Zn}_{0.3}\text{Mn}_{0.7+x}\text{Si}_x\text{Fe}_{2-2x}\text{O}_4$ spinel ferrite series

Kunal B. Modi¹  · Nimish H. Vasoya² · Tushar K. Pathak³ · Pooja U. Sharma⁴ · Komal K. Jani¹ · Priya L. Mange¹ · Pooja Y. Raval⁵ · Kiran G. Saija⁶ · Nisha Thankachen⁷ · Utpal S. Joshi⁷

Received: 3 May 2020 / Accepted: 8 October 2020 / Published online: 18 October 2020
© Springer Nature Switzerland AG 2020

Abstract

A nonvolatile memory effect exhibited by electric field-induced resistance switching has been the topic of intense research not only due to its applications as resistive random access memory but also from the basic physics point of view. Among several binary and ternary mixed oxide compounds, the ones which possess magnetic ions have shown a great promise. Spinel ferrite system $\text{Zn}_{0.3}\text{Mn}_{0.7+x}\text{Si}_x\text{Fe}_{2-2x}\text{O}_4$ with varying x is investigated for its novel electrical switching properties. Both temperature and applied voltage dependence of current-controlled negative resistance-type electrical switching showed better than 200% of resistive switching ratios. Bulk polycrystalline samples showed composition x dependence of resistive switching. The current–voltage characteristics are modeled for low and high applied field regime, and the presence of space-charge-limiting current is confirmed. Thin films of the ferrite system grown by pulsed laser deposition showed almost nonexistence of resistive switching, suggesting that the bulk composition of the compound has a major role to play against the film–electrode interface.

Keywords Spinel ferrite · Electric switching · Space-charge-limiting current · Thin film

1 Introduction

In search of novel memory devices in the modern semiconductor industry, the resistive random access memory (RRAM) has shown a great promise. Despite several complex systems exhibiting promising RRAM behavior, the governing mechanism of electrical switching observed in materials, either the bulk or films, is still under debate. An in-depth analysis of the current–voltage (I – V) characteristics of materials is key in discussing the mechanism of RRAM. Owing to the existence of charge carriers produced thermally, the I – V characteristics of most materials in a small applied electric field are Ohmic (linear) in nature. With the increasing electric field, I – V behavior begins to

be non-Ohmic in the majority of nonmetallic substances. A rapid increase in I with sufficiently high V makes the characteristics nonlinear or rather an exponential dependence near to the electronic breakdown of the material. In certain compounds, the I increases in a linear manner up to a specific applied field and beyond that huge current flows with V abruptly decrease. The mechanism in which materials demonstrate a sudden changeover from high conduction state to low conduction state is referred to as resistive switching (RS). There are three types of RS, namely (a) negative resistance controlled by a voltage (VCNR) or N-type, (b) negative resistance controlled by current (CCNR) or S-type and (c) bi-stable or memory switching.

✉ Kunal B. Modi, kunalbmodi2003@yahoo.com | ¹Department of Physics, Saurashtra University, Rajkot 360005, India. ²Department of Balbhavan, Children's University, Sector-20, Gandhinagar 382021, India. ³Government Engineering College, Mavdi-Kankot Road, Rajkot 360005, India. ⁴Department of Physics, Government Science College, Sector-15, Gandhinagar 382015, India. ⁵Department of Physics, C. U. Shah University, Wadhwan City, Surendranagar 363030, India. ⁶Smt. R. P. Bhalodia Mahila College, Upleta 360490, India. ⁷Department of Physics, University School of Sciences, Gujarat University, Ahmedabad 380009, India.



Very recent (2019–2020) review articles describe all the aspects, starting from fundamentals of resistive switching (RS), mechanisms responsible for switching action, fabrication processes, materials properties, etc., of resistive switching devices for nonvolatile RRAM and computing applications [1–9]. Many pure oxide thin film heterostructures, perovskite oxides, metal halide perovskite, manganites, single-crystalline materials, and thin films of chalcogenide semiconductors, organic and hybrid materials including graphene oxide have shown to exhibit resistive switching [1–9]. Mixed metal oxide systems such as ferrites (spinel, garnets, orthoferrites, etc.) exhibiting memory and switching characteristics are of prime significance in the field of digital electronics. In the last couple of years (2018–2020), a very few research reports are available on RS exhibited by spinel ferrites in nanocrystalline [10–12], thin films [13–20], and nanocomposite [21] forms. Interestingly and surprisingly, no work has been reported on RS action demonstrated by bulk polycrystalline ferrite materials. Of course, it is seldom observed phenomenon in such a class of materials. In this sense, the present work is important. On the other hand, quadruple perovskite, calcium-copper-titanate ($\text{CaCu}_3\text{Ti}_4\text{O}_{12}$), and their isomorphous systems, pristine and substituted with different cations in various forms are commonly exhibited room-temperature and high-temperature nonlinear current versus voltage characteristics suitable for varistor applications [22].

In the present investigation, the composition, $\text{Zn}_{0.3}\text{Mn}_{0.7}\text{Fe}_2\text{O}_4$, is selected as parent material and Si^{4+} is chosen for the substitution based on the following facts: (1) from the high-frequency applications' point of view, this composition possesses excellent properties, for instance high initial magnetic permeability, a large value of saturation magnetization, high electric resistivity and low power loss, (2) the substitution of a tetravalent cation such as Si^{4+} lowered eddy current losses and increased the temperature stability, (3) Si^{4+} ions have a tendency to segregate at the grain boundaries and create a low conductivity layer that strongly affects structural, microstructural, magnetic, electric and dielectric properties [23–28]. The recent advancements and emergent curiosity in the RS demonstrated by mixed oxides prompted us to re-examine the classic ferrite system to comprehend the high electric field instability in the multicationic spinel ferrite series, $\text{Zn}_{0.3}\text{Mn}_{0.7+x}\text{Si}_x\text{Fe}_{2-2x}\text{O}_4$.

2 Experimental details

Comprehensive experimental technicalities relating to the synthesis of spinel ferrite series, $\text{Zn}_{0.3}\text{Mn}_{0.7+x}\text{Si}_x\text{Fe}_{2-2x}\text{O}_4$ with $x=0.0, 0.1, 0.2$ and 0.3 , by usual two-step sintering ceramic route, crystalline phase identification as well as

structural parameters determination by analyzing X-ray diffraction patterns are given in previous reports [23, 24].

The scanning electron microscope, model XL-30 ESEM with EDAX (make: Philips, Netherlands) operated at 30 kV, was employed to register energy-dispersive analysis of X-ray spectra. Current (I) against voltage (V) (ranging from 0 to 400 V) measurements were taken using Aplab made (model 7332) high-voltage dc regulated power supply at selected temperatures in the range of 300–673 K. The cylindrically pelletized samples having a diameter of 1.0 cm and thickness of the order of 0.3–0.4 cm were used for I – V characteristic measurements. The faces of the disc sample were polished by rubbing with zero-grade sandpaper and washed in mild hydrochloric acid (HCl) and propanone. Eventually, graphite was applied on both the plain faces of the pellets on which aluminum foil was also put up for perfect electrical contacts.

The high-quality ceramic target (having a 1.8-cm diameter) of $\text{Zn}_{0.3}\text{Mn}_{0.8}\text{Si}_{0.1}\text{Fe}_{1.8}\text{O}_4$ (ZMSFO) ($x=0.1$) composition was intended for pulsed laser deposition (PLD) using Q-switched Nd: YAG laser (Ekspla Co., Model HT-303) having $\lambda=355$ nm. The ferrite thin film was grown on Pt/SiO₂/Si substrates with dimension of 15×15 mm². The laser pulse repetition frequency was kept at 10 Hz, and laser powers were fixed at 1.7 J for the PLD experiment [29]. During the film deposition process, temperature of the substrate was maintained at 973 K and oxygen partial pressure of 1 mTorr was controlled. The ZMSFO film was deposited on the substrate with the aid of a metal shadow mask on an area of 10×15 mm², and film thickness was monitored to be ~ 260 nm. In order to create the top electrode (area 400×300 μm^2), highly pure Ag was evaporated thermally on the active layer of ferrite film through a metal shadow mask. The heterostructure Ag/ZMSFO/Pt/SiO₂/Si was characterized at 300 K by means of grazing incidence X-ray diffraction (GIXRD, PANalytical), atomic force microscopy (AFM) (Nanosurf AG), stylus surface profiler (DekTak. 3.2, Veeco) and I – V characteristics (Keithley 4200 semiconductor characterization system).

3 Results and discussion

The elemental analyses of synthesized compounds of the series, $\text{Zn}_{0.3}\text{Mn}_{0.7+x}\text{Si}_x\text{Fe}_{2-2x}\text{O}_4$ ($x=0.0$ – 0.3), were conducted, and in Fig. 1 the representative EDAX pattern for the composition with $x=0.2$ is displayed. The peaks are well assigned in accordance with the standard positions. The weight percentage (wt%) of various elements determined from the chemical formulae and that from EDAX analysis correspond well mutually. The results summarized in Table 1 confirm the expected stoichiometry without the loss of any ingredient. The peak-to-background (P/B) ratio was found to be large

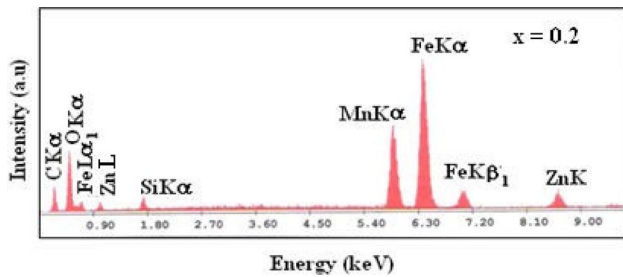


Fig. 1 Typical EDAX pattern for $x=0.2$ composition of the system $Zn_{0.3}Mn_{0.7+x}Si_xFe_{2-2x}O_4$

Table 1 The results of the elemental analysis of $Zn_{0.3}Mn_{0.9}Si_{0.2}Fe_{1.6}O_4$ ($x=0.2$) composition

| Element | EDAX (wt%) ± 2% | Expected (wt%) | (P/B) Ratio |
|---------|--------------------|----------------|-------------|
| Fe | 40.26 | 39.19 | 81.18 |
| Mn | 21.63 | 21.68 | 46.08 |
| Zn | 08.70 | 08.59 | 15.61 |
| Si | 02.45 | 02.46 | 05.66 |
| O | 26.96 | 28.07 | 54.37 |

for the different peaks, so background fitting was free from any inaccuracy.

Precise knowledge of the cation distribution over crystallographic sites in magnetic oxides is highly essential for understanding their physical properties. In order to determine the distribution of metallic cations among the crystallographic interstitial sites, tetrahedral (A-) and octahedral (B-) sites, X-ray diffraction line intensity calculations were performed using the powder $-x$ software [30] and indigenous software [31] based on the formula suggested by Buerger [32]

$$I_{hkl} = |F_{hkl}|^2 \cdot P \cdot L_p \tag{1}$$

where I_{hkl} is the relative integrated intensity, F_{hkl} is the structure factor, P is the multiplicity factor and L_p is the Lorentz polarization factor = $[(1 + \cos^2 2\theta)/\sin^2 \theta \cdot \cos \theta]$. According to Ohnishi and Teranishi [33], the intensity ratios of planes $I(220)/I(440)$, $I(400)/I(422)$, and $I(220)/I(400)$ are considered to be sensitive to any change in cation distribution. The intensities of (220) and (422) planes are mostly sensitive to cations on the tetrahedral sites, while the intensity of (400) plane depends on cations on both the sites. There is a good contrast in the atomic scattering factor of Si^{4+} and Zn^{2+} to that of Fe^{3+} and Mn^{2+} , but the scattering factor of Mn^{2+} is close to that of Fe^{3+} [34]. We had estimated the amount of ferric (Fe^{3+}) ions on the A-site and B-site through low-temperature ($T=80$ K) ^{57}Fe Mossbauer spectral intensity calculations by considering the integrated areas under the Lorentzians corresponding to the A- and B-sites, which were taken as proportional to the amount of Fe^{3+} ion on these sites. The details are given elsewhere [35, 36]. The values of the Seebeck coefficient and absolute ferric ion concentration on the B-sites are further used to calculate ferrous ion (Fe^{2+}) concentration as discussed in [35]. Any alteration in the distribution of cations causes a significant change in the theoretical values of the X-ray diffraction line intensity ratio. Therefore, in the process of arriving at the final cation distribution, the site occupancy of all the cations was varied for many combinations and those that agree well with the experimental intensity ratios, the fitting of the magnetization data at 80 K [26] and Mossbauer data analysis [36] were taken into consideration. The resultant cation distribution and comparison of intensity ratios of planes are shown in Table 2. The percentage accuracy in cationic occupancies is of the order of $\pm 5\%$.

Figure 2 depicts the current (I) against the electric field (E) plots for all compositions registered at various temperatures. It is found that for the pristine composition ($x=0.0$) switching action was recorded at $T_s \geq 373$ K, while for the compositions, $x=0.1, 0.2,$ and $0.3,$ switching was noted, respectively, at $T_s \geq 323$ K, $T_s \geq 473$ K, $T_s \geq 523$ K. In

Table 2 Lattice constant (a), distribution of cations, oxygen deficiency (δ) and microstrain ($\Delta d/d$) for $Zn_{0.3}Mn_{0.7+x}Si_xFe_{2-2x}O_4$ system

| Mn-Si content (x) | a (Å) ± 0.002 Å | Actual cation distribution | $I(400)/I(422)$ | | $I(220)/I(400)$ | | Oxygen deficiency (δ) | $(\Delta d/d) \times 10^{-3}$ |
|-----------------------|----------------------|---|-----------------|-------|-----------------|-------|--------------------------------|-------------------------------|
| | | | Obs | Cal | Obs | Cal | | |
| 0.0 | 8.465 | $(Zn^{+2}_{0.25}Mn^{+2}_{0.40}Fe^{+3}_{0.35}) [Zn^{+2}_{0.05}Mn^{+2}_{0.30}Fe^{+3}_{1.02}Fe^{+2}_{0.63}]O_{3.68}$ | 1.924 | 2.103 | 1.122 | 1.264 | 0.32 | – |
| 0.1 | 8.488 | $(Zn^{+2}_{0.25}Si^{+4}_{0.10}Mn^{+2}_{0.43}Fe^{+3}_{0.22}) [Zn^{+2}_{0.05}Mn^{+2}_{0.37}Fe^{+3}_{1.49}Fe^{+2}_{0.09}]O_{3.95}$ | 2.107 | 2.257 | 0.992 | 1.052 | 0.05 | 1.3515 |
| 0.2 | 8.497 | $(Zn^{+2}_{0.25}Si^{+4}_{0.15}Mn^{+2}_{0.45}Fe^{+3}_{0.15}) [Zn^{+2}_{0.05}Si^{+4}_{0.05}Mn^{+2}_{0.45}Fe^{+3}_{1.36}Fe^{+2}_{0.09}]O_{3.95}$ | 2.071 | 2.191 | 1.294 | 1.206 | 0.05 | 1.8805 |
| 0.3 | 8.505 | $(Zn^{+2}_{0.25}Si^{+4}_{0.21}Mn^{+2}_{0.48}Fe^{+3}_{0.06}) [Zn^{+2}_{0.05}Si^{+4}_{0.09}Mn^{+2}_{0.52}Fe^{+3}_{1.24}Fe^{+2}_{0.10}]O_{3.95}$ | 1.800 | 1.951 | 1.066 | 1.189 | 0.05 | 2.3705 |

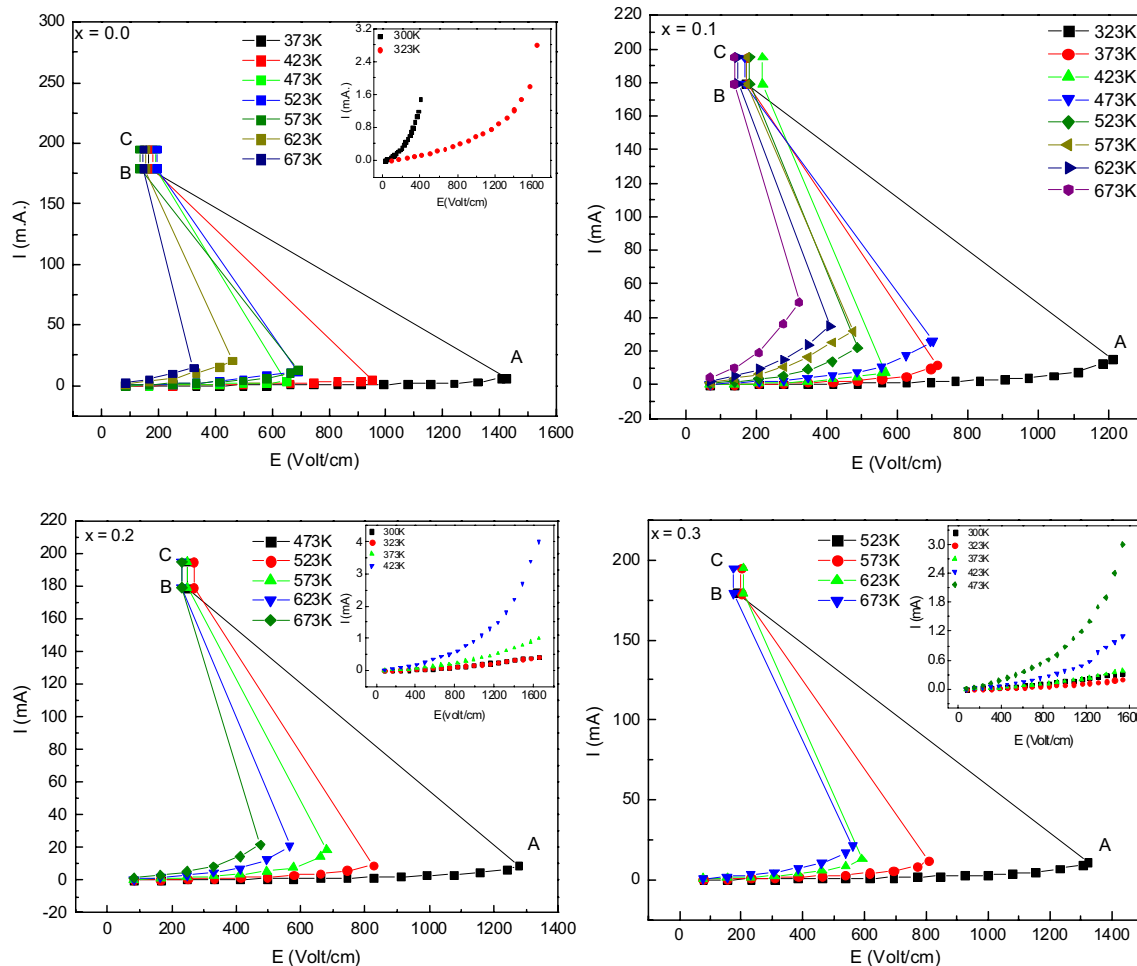


Fig. 2 Current (I) against electric field (E) characteristics for $x=0.0$ – 0.3 compositions registered at selected temperatures

accordance with T_s , electric field strength (E_s) required for switching action to takes place is found to be 1416 V/cm for $x=0.0$ composition, while for $x=0.1$, 0.2 and 0.3 compositions E_s is found to be 1206 V/cm, 1276 V/cm and 1321 V/cm, respectively. In short, T_s and E_s increase with Mn–Si content (x) for $x \geq 0.1$. According to Vaingankar et al. [37], electrical switching is influenced by structural and microstructural parameters. The observed increase in the lattice parameter with x (Table 2) implies that charge carriers require more amount of energy to transfer from one cationic site to another. Thus, the observed increase in T_s and E_s may be correlated with a subsequent increase in the unit cell dimension. The compositional variation of lattice constant has clearly implied that in the system greater proportion of Si^{4+} ions residing at the grain boundaries, while a small quantity did indeed enter into the crystal lattice [24, 26]. Earlier, it has been shown in the case of W-type barium ferrite ($\text{BaCo}_{1.3}\text{Zn}_{0.7}\text{Fe}_{16}\text{O}_{27}$) that grain boundary occupancy of Si^{4+} ions is 5–10 times greater than Si^{4+} ions residing inside the grains [38]. Our results

are consistent with these findings. The presence of silicon ions at the grain boundaries forms a low-conductivity layer as addressed above. Thus, on increasing the concentration (x) intragranular flow of charge carriers get restricted, which turns out in observed increase in E_s and T_s with content (x). Earlier, in the case of the $\text{Cd}_x\text{Co}_{1-x}\text{Fe}_{2-y}\text{Cr}_y\text{O}_4$ spinel ferrite system, it was reported that the switching field (E_s) decreases with a decrease in grain size (D) [14]. In the present case, an average grain size reduces from 12 μm ($x=0.0$) to 6 μm ($x=0.3$) [28], but at the same time E_s is found to increase with (x). This contradicts the previous results.

A careful examination of Fig. 2 revealed the nature of the switching performance. The deviation from the Ohm's law becomes more prominent with an increase in V across the sample when the E is just beyond the value designated by 'A'. During the first cycle, the breakdown abruptly takes place and the field drops to the value marked by B, specified as the first breakdown field; hereafter, the I increases monotonously, from B to C. The aggregate resistance

switching ratio ($R_{\text{high}}/R_{\text{low}}$) approximated for the different compositions is better than 200% at the respective T_s .

The aggregate ON-state current is noted to be ~ 179 mA at the distinct temperatures for all the compositions. It is interesting to note that the switching performance of the samples remains unchanged even when the cycle was performed again after 2 weeks indicating the absence of the 'aging effect.' On the other hand, when the ferrites were under the second switching cycle that was running later than the first cycle, it was observed that the lower value of the electric field is needed for breakdown to take place. This leads to the occurrence of Joule self-heating.

As discussed above, the large class of oxide systems exhibits this interesting phenomenon. Thus, it is difficult to pinpoint any precise reason as being responsible for electrical switching and it may be different for the different systems. Commonly, oxide series containing Jahn–Teller (JT) ions (Mn^{3+} and Cu^{2+}) are the most probable candidates expected to demonstrate switching actions [39].

The series $\text{Zn}^{+2}_{0.3}\text{Mn}^{+2}_{0.7+x}\text{Si}^{+4}_x\text{Fe}^{+3}_{2-2x}\text{O}^{-2}_4$ is fundamentally free from JT ions. Thus, the observed switching action cannot be ascribed to JT ions as suggested. The structural transformation observed [37] likewise cannot be admitted as the origin of this action, as neither of these ferrites demonstrated such transformation in structure as a function of temperature, which otherwise would have been observed in thermal variation of two-probe dc conductivity measurements [26]. The oxygen deficiency (δ), which is customary in aforesaid ferrites, should be allowed for the possibility, but this is most unlikely as verified by EDAX pattern analysis. Further, thermoelectric power measurements have shown that $\delta=0.05$ remains constant for $x=0.1$ – 0.3 compositions [35] (Table 2). Thus, oxygen deficiency cannot be responsible for observed switching action and corresponding changes in T_s and E_s values. Similar observations of the trivial role of oxygen vacancy on RS have been reported for NiO and perovskite manganite $\text{La}_{0.67}\text{Sr}_{0.33}\text{MnO}_3$ [40, 41]. The formation of JT Mn^{+3} ion is presumably in such systems, and concurrently, the formation of a comparable amount of JT ferrous ions (Fe^{+2}) from ferric ions (Fe^{+3}) is anticipated such that the charge neutrality retains. If switching in the system is accorded to the presence of Mn^{+3} ions in the series, then requisite E_s and T_s showed a decrease with Mn–Si content (x), but the findings show an opposite trend.

In addition, thermoelectric power measurements have also demonstrated that the ferrites under study are n-type semiconducting materials. Consequently, switching owing to the cooperative Jahn–Teller distortions does not appear to be tenable. On examining the cation distribution (Table 2), it is evident that on Mn–Si substitution (x), Fe^{3+} ion concentration decreases from the B-site as well as from the system itself. This restricts the exchange of electron

among Fe^{3+} – Fe^{2+} ions, and as a consequence, the values of E_s and T_s required for switching action increase. When highly magnetic Fe^{3+} ions are replaced by non-magnetic Si^{4+} ions that do not take an active part in the conduction mechanism, that curtails the conduction via the B-site. Additionally, the space-charge-limiting current (SCLC) may also be responsible for observed switching action. As stated in the band theory of insulators, supplemental charge carriers are injected through a metallic electrode via an insulator–metal interface. In Fig. 3, it can be seen that for low-voltage region, up to 2.3 V, the current increases almost linearly, suggesting the slope value of $\log I$ versus $\log V$ curves to be approximately 1 for all the compositions. However, beyond 2.3 V, a sharp increase in the current deviates from the linearity and yields a slope of the curves between 1.8 and 2.8 (Fig. 3), which implies that in the high resistance state the conduction mechanism is static induction current (SIC) or SCLC-type. Similar findings and detailed mechanisms are reported in refs. [29] and [42] for binary and ternary oxide compounds, respectively. In SCLC over the insulating layers, increase in large current takes place when trapping sites in the insulating bulk are fully occupied at a threshold voltage (V_T). By and large, V_T is farther than 200 V in the primary action of RS. Beyond the V_T , I swiftly increases (Fig. 3). The drastic rise in I may be induced by trap charge—SCLC. Thus, when the thermally produced free charge carrier density within the system is higher as compared to the density of charge carrier injected, Ohmic ($I \propto V$) characteristic is noticed. In the manner now being exemplified from the $\log I$ against $\log V$ plots (Fig. 3) which exhibit that at low voltage, I follows Ohm's law, and at breakdown voltage, the slope of the curve increases hinting the presence of SCL current which could be referring to as the possible cause of electric switching [43]. This is also an essential feature of CCNR type of electrical switching. Eventually, the I – E characteristics show gradual switching that can be thought of due to CCNR-type switching. On the other hand, fast switching action may be expected on account of VCNR-type switching. Further, I – E characteristics (Fig. 2) exhibited by all the compositions regardless of ferrimagnetic or paramagnetic in nature and are akin to the ON–OFF characteristics of a silicon-controlled rectifier. At long last, an effort has been made to correlate microstructural parameters [grain size (D) and density of defects (d_D)], similar to that of structural parameters (the lattice constant (a) and cation distribution), with electric parameters, E_s and nonlinearity coefficient (α). The values of α and E_s are deployed to characterize the functioning of a device. It is advisable to have a large value of α to protect the device against any electric surges. The α value determined from standard method [22], for example, increases from $\alpha=2.0$ ($x=0.0$) to $\alpha=2.8$ ($x=0.3$) at $T=523$ K, consistent with the slope

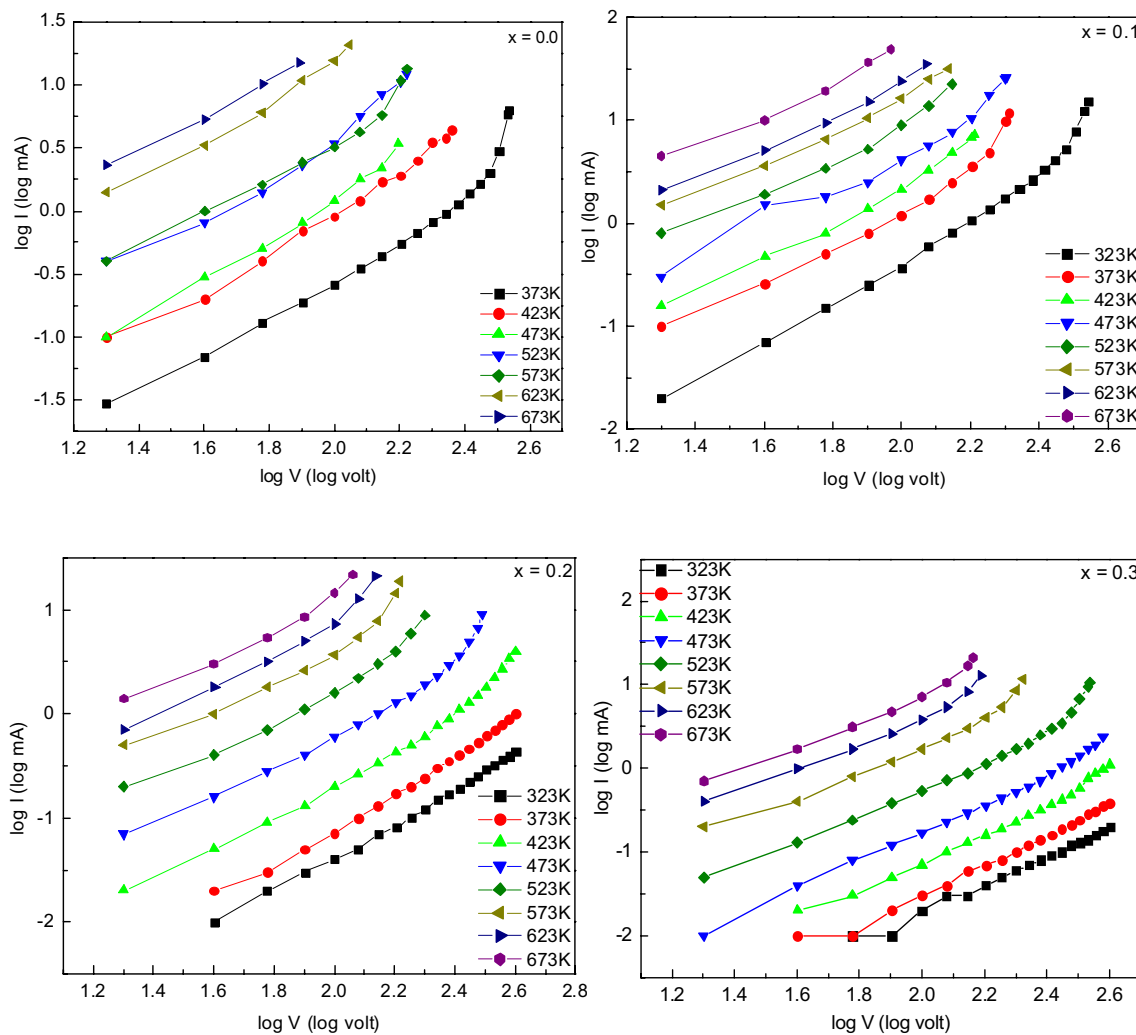


Fig. 3 Temperature dependence of log *I* versus log *V* plots for the Zn_{0.3}Mn_{0.7+x}Si_xFe_{2-2x}O₄ spinel ferrite series

values determined from log *I* versus log *V* plots (Fig. 3), as expected. It has been reported that $d_D \propto 1/D^2 \propto E_s^2$ [22]. On decrease in *D* with content (*x*), d_D is found to increase from $6.94 \times 10^9/\text{m}^2$ for $x=0.0$ composition to $27.8 \times 10^9/\text{m}^2$ for $x=0.3$ composition, suggesting an increase in micro-strain due to the enhancement in tensile force acting on the planes. The variation in lattice microstrain, corresponding to a fractional change in plane spacing, $\Delta d/d$, has been computed for the substituted compositions by taking into account '*d*' spacing value of the most intense (311) peak and is presented in Table 2. This value of $\Delta d/d$, however, comprises both tensile strain and compressive strain and must be divided by a factor of two to get the maximum tensile strain alone, if these two strains are presumed to be the same in strength. Table 1 reveals that strain gradually increases with increasing Mn–Si content (*x*) for $x=0.1$ – 0.3 compositions. A single-peak analysis method [strain determination by the value of $\Delta d/d$ from only (311) reflection] is

based on the assumption that strain broadening is Gaussian, while size broadening is Lorentzian. Other methods analyze the full diffraction pattern, trying to extract the information about the crystallite size and strain based on the different angular dependence of their respective broadening effects. A relatively simple and thus still widely used method is the Williamson–Hall (W–H) plot. This method actually considers the broadening (β) of peaks as a function of a diffraction angle (2θ), which is assumed to be the combined effect of size-induced broadening and strain-induced broadening. In this method, both size and strain broadening are assumed to be Lorentzian, and the integral breadth of both components is additive.

From the W–H plots (Fig. 4), the linear slope gives the value of the lattice strain. It is found that the system Mn_{0.7+x}Zn_{0.3}Si_xFe_{2-2x}O₄ ($x=0.0$ – 0.3) comprises positive and negative values of strain. The positive slope for $x=0.0$ composition suggests the presence of tensile strain

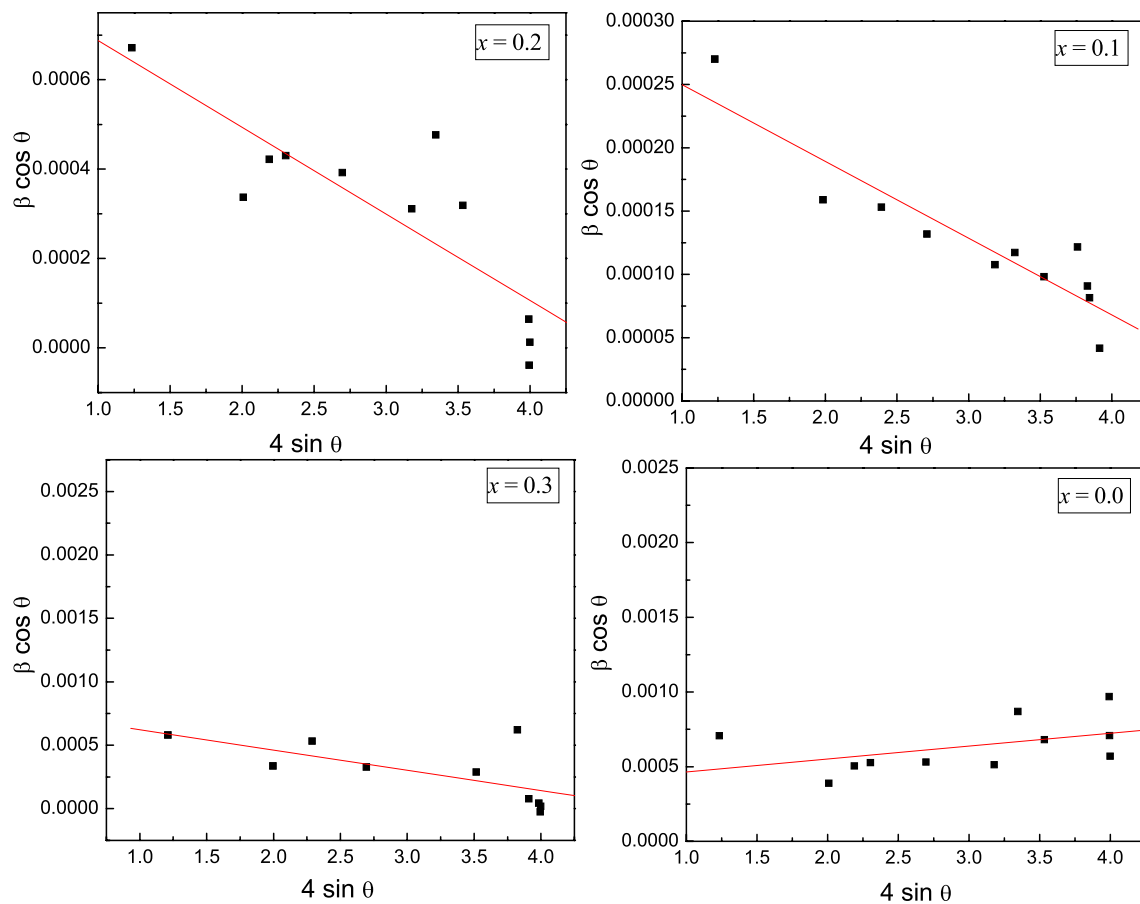


Fig. 4 Williamson and Hall plots for strain determination for all the compositions of the spinel ferrite series $Zn_{0.3}Mn_{0.7+x}Si_xFe_{2-2x}O_4$

(strain = $+0.865 \times 10^{-4}$), whereas the negative slope for $x=0.1, 0.2$ and 0.3 compositions exhibits compressive strain [44] (strain = $-0.606 \times 10^{-4}, -1.59 \times 10^{-4}$ and -1.93×10^{-4} , respectively). All the plots exhibit a scatter point known as a 'deviation pattern,' which is typical of strained cubic materials [45]. The co-substitution of Mn–Si causes significant changes in the structural properties and eventually affects other physical properties. The compressive strain also indicates that microstrains cannot be a dominant source of broadening [46]. On the other hand, in coarse-grained materials, crystallite/grain size has a negligible effect on X-ray diffraction line broadening. The compressive strain increases with increasing content (x) in the system. The variation of strain with x is similar to that of strain determined from single (311) reflection for $x > 0.0$ compositions.

The tensile strain increases owing to the increasing defect density (d_D) as discussed above. Earlier, a detailed role of defects in governing the RS has been reviewed for several oxide thin film systems [47]. Thus, one can expect better nonlinear behavior (higher value of α), as observed. At the same time, as a result, an increase in E_s

with Mn–Si concentration (x) is anticipated as noticed for $x=0.1–0.3$ compositions. These experimental outcomes are of great significance as they bring out the advancement of electric field-induced RS devices.

Figure 5 displays the GIXRD pattern and AFM image of the ZMSFO thin film. The diffraction line analogous to the single face-centered cubic (fcc) phase is clearly seen. The lattice parameter anticipated based on the GIXRD analysis was 8.43 \AA , which is smaller as compared to the bulk counterpart ($a = 8.488 \text{ \AA}$) (Table 2). One or more of the following factors causes the smaller value of unit cell parameter for nanostructured thin film: (1) low degree of crystallinity in nanostructured thin film, (2) the alteration in the site occupancy of cations and (3) the existence of lattice defects that affect the surface of the nanoparticles. Surface energy and tension of the nanoparticles are significant that lead to shrinkage in the lattice, which elicits a reduction in lattice constant [48]. AFM image shows a homogeneous distribution of grains, and the aggregate particle size approximated is varying between 50 and 65 nm. The AFM analysis has shown RMS

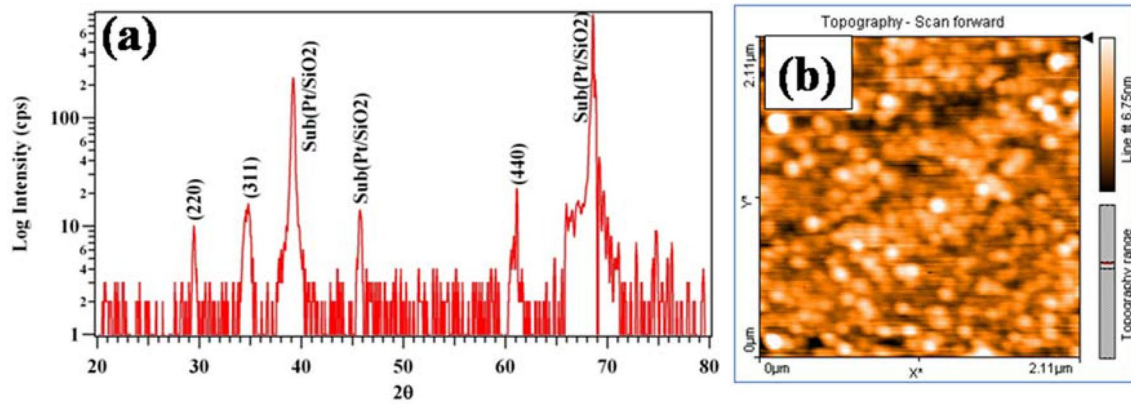


Fig. 5 GIXRD pattern of ZMSFO film grown on Pt/SiO₂/Si substrate. A single cubic phase can be seen (b). Bi-dimensional AFM surface topography of ZMSFO/Pt/SiO₂/Si heterostructure

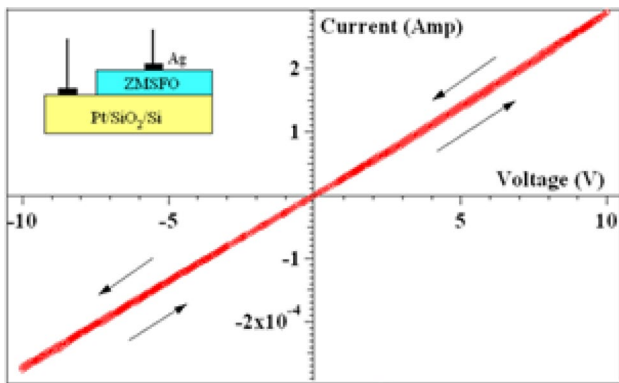


Fig. 6 *I*-*V* characteristics of Ag/ZMSFO/Pt/SiO₂/Si heterostructure. The inset shows the schematic of measurement geometry and arrows indicate typical voltage sweeping cycles

roughness of the order of ~6.8 nm that is equitably modest alluding to even-textured grain morphology.

Figure 6 illustrates *I*-*V* characteristics of Ag/ZMSFO/Pt/SiO₂/Si heterostructure examine by employing the bi-terminal method. The inlay shows a schematic of a cross section of the Ag/ZMSFO/Pt/SiO₂/Si sandwich configuration intended for the *I*-*V* measurements. Figure 6 shows linear *I*-*V* behavior for every cycle of voltage sweeping implying the absence of RS characteristics. These outcomes point out that the electrical transport associated with the interface is most unlikely for the RS phenomenon in the ferrite thin film.

4 Conclusions

In conclusion, spinel ferrite system Zn_{0.3}Mn_{0.7+x}Fe_{2-2x}O₄ (*x* = 0.0–0.3) in its bulk and thin film forms have been studied for its current-controlled negative resistance-type

electrical switching properties. Elevated temperatures and high electric fields are essential parameters along with the Mn–Si concentration (*x*) for the observed enhancement in the electrical switching in the ferrite oxide system. Moreover, the expansion in lattice parameter, abatement of octahedral site occupancy of Fe³⁺ ion in spinel lattice, and partial grain boundaries occupancy of Si⁴⁺ ions may have an important role for the switching characteristics. The modeling of the *I*-*V* data confirmed the presence of space-charge-limiting current, which could be a responsible source of observed switching. The PLD grown ferrite thin film shows linear behavior in current against voltage characteristic without any signature of resistive switching, suggesting that the bulk composition of the compound has a major role to play against the film–electrode interface.

Acknowledgements Ms. P. L. Mange is appreciative of DST-New Delhi for offering monetary assistance under the INSPIRE program. NT thanks IUAC, New Delhi, for a fellowship.

Compliance with ethical standards

Conflict of interest The authors declare that they have no conflict of interest.

References

1. Wang Z, Wu H, Burr GW, Hwang CS, Wang KL, Xia Q, Yang JJ (2020) Resistive switching materials for information processing. *Nat Rev Mater* 5:173–195
2. Romero FJ, Toral A, Medina-Rull A, Moraila-Martinez CL, Morales DP, Ohato A, Godoy A, Ruiz FG, Rodriguez N (2020) Resistive switching in graphene oxide. *Front Mater* 7:17–21
3. Slesazeck S, Mikolajick T (2019) Nanoscale resistive switching memory devices: a review. *Nanotechnol* 30(35):352003

- Li B, Hui W, Ran X, Xia Y, Xia F, Chao L, Chen Y, Huang W (2019) Metal halide perovskites for resistive switching memory devices and artificial synapses. *J Mater Chem C* 7(25):7476–7493
- Lee SH, Zhu X, Lu WD (2020) Nanoscale resistive switching devices for memory and computing applications. *Nano Res* 13:1228–1243
- Munjal S, Khare N (2019) Advances in resistive switching based memory devices. *J. Phys. D. Appl. Phys.* 52(43):433002
- Gao S, Yi X, Shang J, Liu G, Li R-W (2019) Organic and hybrid resistive switching materials and devices. *Chem Soc Rev* 48(6):1531–1565
- Brivio S, Menzel S (2020) Resistive switching memories, Chap. 2. In: *Memristive Devices for Brain-Inspired Computing. From Materials, Devices, and Circuits to Applications - Computational Memory, Deep Learning, and Spiking Neural Networks*. Woodhead Publication 1 Series in Electronics and Optical materials, vol 1. Woodhead Publishing, pp 17–61
- Shen Z, Zhao C, Qi Y, Xu W, Liu Y, Mitrovic IZ, Yang L, Zhao C (2020) Advances of RRAM devices: resistive switching mechanisms, materials and bionic synaptic application. *Nanomaterials* 10:1437–1467
- Kamran M, A-u-Rehman M (2020) Enhanced transport properties in Ce doped cobalt ferrites nanoparticles for resistive RAM applications. *J Alloy Compd* 822:153583
- Munjal S, Khare N (2018) Resistive switching characteristics of monodisperse CoFe_2O_4 nanoparticle assembly. *Adv Sci Lett* 24(2):893–896
- Hasan MS, Arshad MI, Ali A, Mahmood K, Amin N, Ali SS, Khan MI, Mustafa G, Khan MJ, Saleem M (2018) Mg and La co-doped ZnNi spinel ferrites for low resistive applications. *Mater Res Exp* 6(1):016302
- Wu L, Dong C, Wang X, Li J, Li M (2019) Annealing effect on the bipolar resistive switching memory of NiZn ferrite films. *J Alloy Compd* 779:794–799
- Hao A, Jia D, Ismail M, Huang W, Chen R, Bao D (2019) Electric field induced manipulation of resistive and magnetization switching in Pt/NiFe_{1.95}Cr_{0.05}O₄/Pt memory devices. *Appl Phys Lett* 114:203502
- Ismail M, Hao A, He S, Huang W, Qin N, Bao D (2018) Reversible transitions among four modes of nonpolar resistive switching characteristics in nanocrystalline zinc ferrite magnetic thin films. *J Alloy Compd* 753:100–110
- Hao A, Ismail M, He S, Qin N, Chen R, Rana AM, Bao D (2018) Enhanced resistive switching and magnetic properties of Gd-doped NiFe₂O₄ thin films prepared by chemical solution deposition method. *Mater Sci Engg B* 229:86–95
- Yao C, Hu W, Ismail M, Thatikonda SK, Hao A, He S, Qin N, Huang W, Bao D (2019) Coexistence of resistive switching and magnetism modulation in sol-gel derived nanocrystalline spinel Co₃O₄ thin films. *Curr Appl Phys* 19(11):1286–1295
- Hao A, Ismail M, He S, Qin N, Huang W, Chen R, Wu J, Bao D (2018) Improved unipolar resistive switching characteristics of Au-doped nickel ferrite magnetic thin films for non-volatile memory applications. *J Alloy Compd* 732:573–584
- Munjal S, Khare N (2020) AIP conference proceedings. 2220:020171
- Hao AZ, Ismail M, He S, Huang W, Qin N, Bao DH (2018) Coexistence of unipolar and bipolar resistive switching behaviors in NiFe₂O₄ thin film devices by doping Ag nanoparticles. *J Appl Phys* 123:085108
- Tamm A, Joost U, Mikror M, Kalam K, Mandar H, Seemen H, Link J, Stern R, Castan H, Duenas S, Kukli K (2017) Properties of zirconium oxide and cobalt ferrite layered nanocomposite. *ECS J Solid Stat Sci Tech* 6(12):P886–P892
- Raval PY, Makadiya AR, Pansara PR, Sharma PU, Vasoya NH, Bhalodia JA, Kumar S, Dolia SN, Modi KB (2018) Effect of theory on structural microstructural properties and J-E characteristics of CaCu₃Ti₄O₁₂ polycrystalline ceramic. *Mater Chem Phys* 212:343–350
- Vasoya NH, Jha PK, Saija KG, Dolia SN, Zankat KB, Modi KB (2016) Electric modulus, scaling and modeling of dielectric properties of Mn²⁺-Si⁴⁺ co-substituted Mn-Zn ferrites. *J Elect Mater* 45(2):917–927
- Vasoya NH, Jha PK, Saija KG, Bhalodia JA, Modi KB (2017) Master curve generation and modeling of ac conductivity for Mn_{0.7+x}Zn_{0.3}Si_xFe_{2-2x}O₄ spinel ferrite system. *J Adv Diele* 7(03):1750022
- Vasoya NH, Saija KG, Dolia SN, Jha PK, Modi KB (2017) Impedance spectral analysis and scaling behaviour of Mn²⁺-Si⁴⁺ substituted Mn-Zn ferrites. *Mater Res Exp* 4(11):116301
- Saija KG, Vasoya NH, Modi SK, Meshiya UM, Jani KK, Raval PY, Modi KB (2020) Bulk magnetization temperature dependent ac susceptibility and dc resistivity study on Mn_{0.7+x}Zn_{0.3}Si_xFe_{2-2x}O₄ (x = 0.0–0.3) spinel ferrites. *Phys B Condens Matter* 593:412302
- Vasoya NH, Saija KG, Makadiya AR, Meshiya UM, Raval PY, Modi KB (2020) Dielectric relaxation and suitability of scaling parameters study on Mn_{0.7+x}Zn_{0.3}Si_xFe_{2-2x}O₄ (x = 0.0–0.3) ferrites. *Adv Mater Lett*. <https://doi.org/10.5785/amlett.2020.xxxx>
- Saija KG, Raval PY, Joshi NP, Makadiya AR, Kathad CR, Modi SK, Vasoya NH, Modi KB (2020) Permeability spectral analysis and determination of microstructural parameters for Mn_{0.7+x}Zn_{0.3}Si_xFe_{2-2x}O₄ series. *J Supercond Nov Magn* 33(9):8
- Mistry BV, Pinto R, Joshi US (2015) Memristive properties of In₂O₃/LaNiO₃ heterostructures grown by pulsed laser deposition. *J Mater Sci Mater Elect* 27(2):1812–1816
- Dong C (1999) Powder-X Windows-95 based program for powder X-ray diffraction data processing. *J Appl Cryst* 32:838
- Tanna AR, Joshi HH (2013) Computer aided X-ray diffraction intensity analysis for spinels: hands—on computing experience. *Proc World Acad Sci Engg Tech* 7(3):334–341
- Buerger MJ (1960) *Crystal structure analysis*. Wiley, NY
- Ohnishi H, Teranishi T (1961) Crystal distortion in copper ferrite chromite series. *J Phys Soc Jpn* 16:35
- Cullity BD (1978) *Elements of X-ray diffraction*, 2nd edn. Addison Wesley Pub. Co., Reading MA
- Saija KG (2012) Ph. D. thesis, Suarashtra University, Rajkot, India
- Saija KG, Modi KB (unpublished work)
- Vasambekar PN, Kolekar CB, Vaingankar AS (1999) Electrical switching in Cd_xCo_{1-x}Fe_{2-y}Cr_yO₄ system. *Mater Res Bull* 34(6):863–868
- Wu Y, Li ZW, Chen L, Wang SJ, Ong CK (2004) Effect of doping SiO₂ on high-frequency material properties of W-type barium ferrite. *J Appl Phys* 95(8):4235–4239
- Yamashiro T (1973) Electrical switching and memory phenomena in CuFe₂O₄. *Jap J Appl Phys* 12(1):148–149
- Joshi US, Trivedi SJ, Bhavsar KH, Trivedi UN, Khan SA, Avasthi DK (2009) Resistance switching properties of planner Ag/Li: NiO/Ag structures induced by swift heavy ion irradiation. *J Appl Phys* 105(7):73704
- Bhavsar KH, Joshi US, Mistry BV, Khan SA, Avasthi DK (2011) Memristive switching induced by 100 MeV Ag⁺⁷ ion irradiation in planar Ag/La_{0.7}Sr_{0.3}MnO₃/Ag structures. *Rad Eff Def Solids* 166(8–9):718–724
- Pandya NC, Debnath AK, Joshi US (2015) Resistance switching and memory effects in solution-processed BiFeO₃/LaNiO₃ junctions. *J Phys D Appl Phys* 49(5):055301
- Sze SM, Ng KK (2006) *Physics of semiconductors devices*, 3rd edn. Wiley, New Delhi, p 586
- Routray KL, Behera D (2018) Enhancement in conductivity and dielectric properties of rare-earth (Gd²⁺) substituted nanosized CoFe₂O₄. *J Mater Sci* 29(16):14248–14260

45. Vasoya NH, Vanpariya LH, Sakariya PN, Timbadiya MD, Pathak TK, Lakhani VK, Modi KB (2010) Synthesis of nanostructured material by mechanical milling and study on structural property modifications in $\text{Ni}_{0.50}\text{Zn}_{0.50}\text{Fe}_2\text{O}_4$. *Ceram Int* 36:947
46. Langford JI, Cernik RJ, Louer D (1991) The breadth and shape of instrumental line profiles in high resolution powder diffraction. *J Appl Cryst* 24(5):913–919
47. Joshi US (2011) Ion irradiation: a tool to understand oxide RRAM mechanism. *Rad Eff Def Solids* 166(8–9):724–733
48. Chhaya UV, Mistry BV, Bhavsar KH, Gandhi MR, Lakhani VK, Modi KB, Joshi US (2011) Structural parameters and resistive switching phenomenon study on $\text{Cd}_{0.25}\text{Co}_{0.75}\text{Fe}_2\text{O}_4$ ferrite thin film. *Ind J Pure Appl Phys* 49:833–840

Publisher's Note Springer Nature remains neutral with regard to jurisdictional claims in published maps and institutional affiliations.